X-ray Photoelectron Spectroscopy of Fast-Frozen Hematite Colloids in Aqueous Solutions. 3. Stabilization of Ammonium Species by Surface (Hydr)oxo Groups

ARTICLE *in* THE JOURNAL OF PHYSICAL CHEMISTRY C · MARCH 2011

Impact Factor: 4.77 · DOI: 10.1021/jp2002035

3 AUTHORS, INCLUDING:

Kenichi Shimizu
University of Oxford
17 PUBLICATIONS **311** CITATIONS
SEE PROFILE

Jean-Françoi Boily
Umeå University
87 PUBLICATIONS **1,648** CITATIONS
SEE PROFILE

THE JOURNAL OF PHYSICAL CHEMISTRY C

ARTICLE

pubs.acs.org/JPCC

X-ray Photoelectron Spectroscopy of Fast-Frozen Hematite Colloids in Aqueous Solutions. 3. Stabilization of Ammonium Species by Surface (Hydr)oxo Groups

Kenichi Shimizu, Andrei Shchukarev, and Jean-François Boily*

Department of Chemistry, Umeå University, SE-901 87, Umeå, Sweden

Supporting Information

ABSTRACT: The speciation of ammonium at the hematite/water interface was probed by cryogenic X-ray photoelectron spectroscopy. Wet pastes of colloidal hematite spheroids equilibrated in aqueous solutions of 50 mM NH_4Cl exhibit distinctive pH-sensitive N 1s peaks for both NH_4^+ (401.7 eV) and NH_3 (400.1 eV), yet total N/Fe ratios remain relatively invariant (0.029 ± 0.006) throughout the pH 2.2−10.5 range. Both NH_4^+ and NH_3 species coexist throughout most of the tested pH range. NH_4^+ is most likely stabilized at the interface by hydrogen bonding with surface (hydr)oxo groups. A cationic sorption edge for NH_3 is driven by proton abstraction of NH_4^+ by (hydr)oxo groups, forming surface complexes of the type ≡Fe−OH···NH_3. These interactions shift the NH_4^+/NH_3 equilibrium from pK_a = 9.3 in water to 8.4 at the interface. Removal of excess water by vacuum dehydration induces, on the other hand, formation of NH_2 directly bound to surface Fe atoms. These results underscore distinct ammonium species in contact with mineral surfaces and should be considered in understanding environmental and catalytic reactions in this medium.

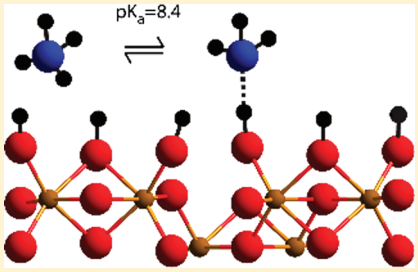

1. INTRODUCTION

Mineral/water interfaces play important roles in environmental and technological settings. Interactions between metal oxides and electrolyte ions are central to this matter and can affect surface charge development, coordination, ion exchange, water exchange, and thereby catalytic reactivity.[1,2] A fundamental understanding of electrolyte ion binding is consequently essential for prediction of environmental proceses and optimization of technological processes.

Interactions of electrolyte ions with metal oxide surfaces are controlled by electrostatic and solvation contributions.[3] The latter expresses the propensity of ions and mineral surfaces in sharing or exchanging hydration water molecules, stabilized by hydrogen bonding. Solvation energy contributions in electrolyte adsorption are, therefore, more significant for ions with higher affinities toward water. Of the several inorganic electrolyte ions ubiquitous to environmental and technological settings, the ammonium ion is of high interest.[4−7] This ion lies on top of the Hofmeister series of cations for its water-breaking properties, notably seen through low mean residence time of first hydration shell molecules. Its solvation environment is highly flexible and cooperative and enables rapid translational and rotational motions. (Hydr)oxo groups of metal oxide surfaces can also interact with the ammonium ion through hydrogen bonding or alternatively take part in ligand exchange reactions, resulting in covalently bonded ammonia species with surface metal ions.[8−11] Although sorption mechanisms have been more clearly elucidated in the gas phase, processes taking place in contact with aqueous media, where ammonium ion is a dominant background electrolyte, are not as clearly elucidated. A thorough understanding of such interactions is relevant not only to fundamental aspects of the aqueous and interfacial chemistries of ammonium but also to the study of nitrogen-based fertilizers in the environment and in improving ammonia utilization in hydrogen fuel production.

Isolation of the genuine metal oxide/water interface from bulk solution has long been posed by numerous difficulties. Several X-ray techniques have in a large part circumvented many such problems and started providing insights into the nature of metal oxide−electrolyte interactions.[12−14] Cryogenic X-ray photoelectron spectroscopy (XPS) has notably contributed to these efforts by enabling quantitative measurements of electrolyte loadings on metal (oxy)(hydr)oxide surfaces.[15−19] This technique has recovered pH and ionic strength dependences of electrolyte binding to minerals including goethite,[17] hematite,[15,16,18] gibbsite,[17] and manganite.[19] Of these, hematite (α-Fe_2O_3) has been the object of more intense investigations in our laboratory these past years due to its importance in electron transfer processes in natural and technological settings. We have notably uncovered hydrated NaCl salts on predominantly neutrally charged hematite particles[15] and applied a thermodynamic adsorption model to predict Na^+ and Cl^- adsorption on other hematite colloids.[16] In this study we extend these efforts to the ammonium ion and highlight a markedly different sorption behavior compared to other electrolyte ions.

Received: January 7, 2011
Revised: February 24, 2011
Published: March 16, 2011

2. MATERIALS AND METHODS

2.1. Chemicals and Materials. Ferric chloride and ammonium chloride (ACS/ISO grade) were obtained from Merck (pro analysi). Hydrochloric acid was of VWR (analytical grade Briare), and aqueous ammonia was obtained from Scharlau Chemie (25%, reagent grade, Sentmenat). Doubly distilled deionized water was filtered through Milli-Q plus 185, QPAK purification pack (lot #F9MN39572), and nitrogen gas was humidified and further purified by passing through traps of deionized water and 0.1 M NaOH. Synthetic hematite was dialyzed with Spectra/Pro molecular porous membrane tubing (MWCO: 12000−14000, Spectrum Laboratories). Solution pH was measured with a glass electrode (Orion 8103SC), calibrated daily using pH buffers (pH 3, 4, 7, and 9).

2.2. Hematite Synthesis and Characterization. Hematite was synthesized using the forced hydrolysis method.[20] A 0.72 M $FeCl_3$ solution was added dropwise to a vigorously stirred 3 mM HCl solution preheated to 100 °C. The resulting mixture was then matured at 100 °C for 7 days. The freshly prepared hematite suspension was thereafter dialyzed until the supernatant resistivity exceeded 10^6 Ω·cm. The resulting hematite suspension was diluted with doubly distilled deionized water to a concentration of 4.32 g/L.

Powder X-ray diffraction spectroscopy was conducted on hematite dried in an oven at 80 °C. The solids were ground to powder with a mortar and pestle before loading. The diffraction angle was swept from 20° to 80° at 0.008°/s. The diffraction pattern confirms the rhombohedral structure indicative of a structurally pure hematite.[21] The crystallite size of hematite derived from the X-ray diffractogram (32 nm) is in agreement with transmission electron microscopy images (Figure S1 of Supporting Information; 36 nm, based on 10 spheroidal particles). Assuming spherical particles, diameters within d = 32−36 nm would correspond to specific surface area of 32−36 m^2/g ($6 \cdot d^{-1} \cdot \rho_s^{-1}$; ρ_s is the specific gravity of hematite). These values are in close agreement with our experimental BET surface area of 39.8 m^2/g and, alongside BHJ adsorption pore values (0.0104 cm^3/g and 1.077 nm), suggest surfaces of low porosity. Finally, sample purity with respect to carbon and co-ions used in the synthetic procedure (Figure S2−S3) was confirmed by XPS of dried and fast frozen samples.

2.3. Cryogenic XPS. All XPS spectra were recorded with a Kratos Axis Ultra electron spectrometer equipped with a delay line detector. A monochromated Al Kα source operated at 150 W, a hybrid lens system with a magnetic lens, providing an analysis area of 0.3 mm × 0.7 mm, and a charge neutralizer were used for the measurements. The binding energy (BE) scale was adjusted with respect to the C 1s line of aliphatic carbon, set at 285.0 eV. All spectra were processed with the Kratos software.

Aliquots of 3−6 mL of 50 mM NH_4Cl stock suspensions were purged with N_2(g) overnight in 15 mL polyethylene tubes in a room thermostatted at 25 °C. Suspension pH was then adjusted between 2.2 and 10.5 by addition of HCl and NH_4OH. The samples were equilibrated until the electromotive force of the glass electrode drifted less than 0.3 mV/min and were then centrifuged at 4000 rpm for 15 min. The wet hematite pastes were thereafter transferred onto a XPS sample holder of the transfer rod air-lock, precooled to −170 °C. The sample was kept under dry N_2(g) for 45 s to ensure freezing prior to activating a vacuum to 10^{-7} Torr. The frozen paste was then transferred to the precooled manipulator for XPS analysis at −150 °C and 10^{-9} Torr. One sample at pH 6.2 was also dried in vacuo overnight by removing the cold source, without altering the sample position in the analysis chamber. The resulting dry sample was analyzed by XPS at room temperature to provide information on chemical transformations associated with water loss and formation of oxygen-deficient hematite surfaces.

Survey spectra were collected from 1100 to 0 eV at pass energy of 160 eV. High-resolution spectra (pass energy 20 eV) for Fe 2p, O 1s, N 1s, C 1s and Cl 2p were in turn collected at 0.1 eV/step. Acquisition times for N 1s and Cl 2p spectra in fast-frozen hematite pastes ranged from 60 to 90 min, while those for an aqueous sample (pH 8.4) only required 15 min for achievement of acceptable signal-to-noise ratios. All high-resolution XPS spectra were processed using Shirley backgrounds, and peaks were modeled using a 70% Gauss/30% Lorentz function. Peak positions and full width at half-maximum (fwhm) are reported in Table 1

2.4. Chemometric Analyses. Chemometric analyses of Shirley background-subtracted N 1s spectra were conducted as an additional independent validation of the spectral fits. A $m \times n$ matrix of normalized intensities ($\mathbf{X}$) over m binding energies for n spectra was used to determine the number of linearly independent factors accounting for the variance of the data. A singular value decomposition (SVD) of this matrix, $\mathbf{X} = \mathbf{USV}^T$, produced orthogonalized abstract vectors of unit length in matrix $\mathbf{U}$, their corresponding lengths in matrix $\mathbf{S}$, reported in decreasing values, and factor loadings in the transposed (T) matrix $\mathbf{V}$. The factor indicator function[22] (IND) was used to identify the first k vectors associated to the spectral attributes of N

$$\mathrm{IND} = \mathrm{RSD}(k)/(n-k)^2 \quad (1)$$

where RSD(k) is the residual standard deviation from the misfit of the product $\mathbf{U}_{n\times k}\mathbf{S}_{k\times k}\mathbf{V}_{k\times m}{}^T$ to $\mathbf{X}$. The *inverse* of this function increases monotonically with k and reaches a clear maximum at its optimal value, K. The product $\mathbf{X}_{net} = \mathbf{U}_{n\times K}\mathbf{S}_{K\times K}\mathbf{V}_{K\times m}{}^T$, using the optimal K vectors, contains all chemically relevant contributions of the experimental data. The residual $\mathbf{E} = \mathbf{X} - \mathbf{X}_{net}$ contains, on the other hand, the extractable error,[22] which includes instrument noise and manipulation errors.

Abstract vectors $\mathbf{U}_{n\times K}$ were rotated into a real chemical space to produce spectral components ($\boldsymbol{\varepsilon}_{n\times k}$), akin to extinction coefficients in optical spectroscopy, and an associated concentration profile ($\mathbf{C}_{k\times m}$) for nitrogen species. The product $\mathbf{X}_{net,\,model} = \boldsymbol{\varepsilon}\mathbf{C}$ was used to reproduce $\mathbf{X}_{net}$ by search of optimal values of $\boldsymbol{\varepsilon}$ and $\mathbf{C}$. We have already employed this strategy on a number of systems (aqueous, solids, surfaces) and spectroscopic methods (XPS, FTIR, UV−vis spectrophotometry, X-ray total scattering) using a variety of numerical approaches.[23−28] The one that lends itself best to surface speciation problems involves a model-free multivariate curve resolution (MCR) strategy to avoid constrainment of $\mathbf{C}$ to strictly predefined thermodynamic functions. This was carried out using the program MCR-ALS (v. 1.0.0)[29] which, for this study, produced K spectral components by rotation of the first K abstract vectors $\mathbf{U}$. All calculations were carried out in the computational language of Matlab (The Mathworks, Inc.).

3. RESULTS AND DISCUSSION

Peak-fitting results of the N 1s (Figure 1), Fe 2p (Figure 2a), O 1s (Figure 2b), and Cl 2p (not shown) regions are reported in Tables 1 and 2. As initially shown in the previous papers of this series,[15,16] Fe 2p (Figure 2a) and O 1s (Figure 2b) regions are

dx.doi.org/10.1021/jp2002035 |J. Phys. C 2011, 115, 6796–6801

Table 1. Binding Energies (eV)[a]

	Fe $2p_{3/2}$		O 1s			N 1s		Cl 2p
sample	Fe #1	Fe #2	O	OH	H_2O	NH_3	NH_4	$2p_{3/2}$
				No NH_4Cl				
dry hematite	709.8	711.1	530.0(1.0)	531.4(1.2)	532.6(1.5)			198.5(1.2)
wet	709.9	711.2	530.0(1.0)	531.2(1.5)	533.3(1.8)			198.0(1.3)
				Fast-Frozen in 50 mM NH_4Cl				
pH 2.2	709.8	711.2	530.0(0.9)	531.1(1.5)	533.3(1.5)	399.9(1.5)	401.7(1.8)	198.2(1.1)
pH 4.2	709.9	711.1	530.0(0.9)	531.2(1.4)	533.2(1.6)	400.1(1.4)	401.8(1.8)	198.3(1.1)
pH 6.2	709.8	711.2	530.0(0.9)	531.2(1.4)	533.2(1.4)	400.0(1.5)	401.7(1.7)	198.3(1.0)
pH 8.4	709.9	711.2	530.0(0.9)	531.3(1.2)	533.3(1.6)	400.1(1.3)	401.8(1.8)	198.2(1.1)
pH 10.5	709.9	711.2	530.0(0.9)	531.3(1.4)	533.2(1.9)	400.1(1.5)	401.8(1.8)	198.3(1.1)
				Dried in Vacuo				
pH 6.2	709.9	710.9	530.0	531.5	532.4	400.2	398.5 (NH_2)	198.5

[a] FWHM are shown in parentheses, where relevant. Binding energies are referenced to O1s oxide at 530.0 eV. The entire 701−737 eV region was used for Fe determination. Only the dominant 709.9 (Fe#1) and 711.2 (Fe#2) eV peaks are reported here. "Dry" and "wet" samples do not contain NH_4Cl but only residual chloride from the synthetic procedure.

representative of hematite in contact with frozen water. The characteristic dove-tailed multiplet structure of hematite, with predominant peaks at 711.1−711.2 and 709.8−709.9 eV,[30] are invariable in all samples. The 719.5 eV satellite moreover confirms that iron is present as Fe(III) and that, therefore, the 709.9 eV peak is not from Fe(II). The O 1s region is dominated by structural O and nonstoichiometric OH peaks. Dry samples (with and without NH_4Cl) are depleted in oxygen (O_{Total}/Fe = 1.25 and 1.14; Table 2) due to removal of surface OH and H_2O to the vacuum. Wet samples retain, on the other hand, near stoichiometric O/Fe ratios (1.48−1.69) (Figure 3b), consistent with the predominance of oxygen-terminated surfaces (structural O, surface OH, H_2O). Interestingly, the sample reacted in deionized water contains twice the water content than samples reacted in 50 mM NH_4Cl, a result pointing to a thinning of the interfacial region by these electrolyte ions. In NH_4Cl-bearing pastes, Cl 2p peaks are strongly affected by pH and achieve Cl/Fe loadings (Figure 3a) comparable to previously studied chloride-bearing solutions.[16] These loadings result from physisorbed, and potentially chemisorbed, chloride ions required to neutralize surface charge.[16] Total N/Fe loadings (0.029 ± 0.006 N/Fe) are, on the other hand, relatively unaffected by pH (Figure a). Systematic changes in intensities of two dominant peaks centered at 401.7 ± 0.1 and 400.0 ± 0.1 eV, however, point to important variations in N speciation in this system.

The N 1s region was first modeled as linear combinations of two Gauss−Lorentz (70:30) components with peaks centered at binding energies characteristic of NH_4^+ (401.7 ± 0.3 (3σ) eV) and NH_3 (400.0 ± 0.4 (3σ) eV) species.[8,31] No additional peaks could be extracted from these analyzes. Relative peak areas vary systematically over the pH 2.2−10.5, reaching equal values at pH 8.4 (Figures 1b, 4). The spectrum of a 50 mM NH_4Cl solution at pH 8.4 (Figure 1b) is, in contrast, dominated by the NH_4^+ species. This difference therefore supports stabilization of ammonia in the hematite paste, relative to aqueous solutions. Similar effects were also observed for *N*-(phosphonomethyl)glycine on goethite[32] and bayerite[33] and amino acids on bone graft substitute materials.[34]

Our peak-fitting results are also supported by independent chemometric analyses of the same data set. The IND function[29]

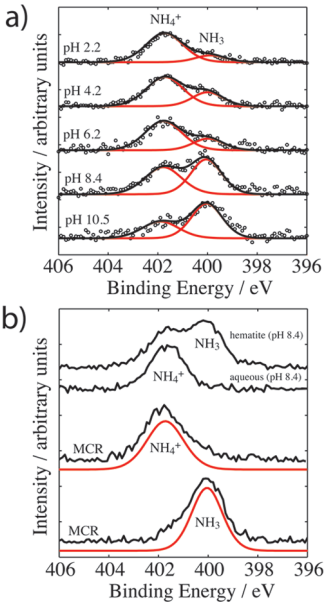

Figure 1. (a) Cryogenic XPS spectra (−170 °C) of hematite wet pastes equilibrated in 50 mM NH_4Cl (25 °C) at pH 2.2, 4.2, 6.2, 8.4, and 10.5. Gauss−Lorentz (70:30) functions (red lines) and their sums as black lines. (b) Top two spectra highlight important speciation changes on hematite compared to an aqueous solution at the same pH (8.4). MCR components (black lines) extracted from the pH 2.2−10.5 spectra for NH_4^+ and NH_3 are shown in the bottom two spectra compared to Gauss−Lorentz (70:30) functions (red lines).

reveals an optimal number of $K = 2$ components (Figure S4) that can be used to adequately reproduce the experimental data. Consistent with these findings, MCR-ALS analyses could only extract two chemically relevant spectral components (Figure 1b). Attempts at fitting the spectra with more than two components provided no significant improvement to the fit of the data. Additional components had moreover physically unrealistic spectral shapes and insignificant values of **C**. Our two MCR components are comparable to those peak-fitting analyses

dx.doi.org/10.1021/jp2002035 |*J. Phys. Chem. C* 2011, 115, 6796–6801

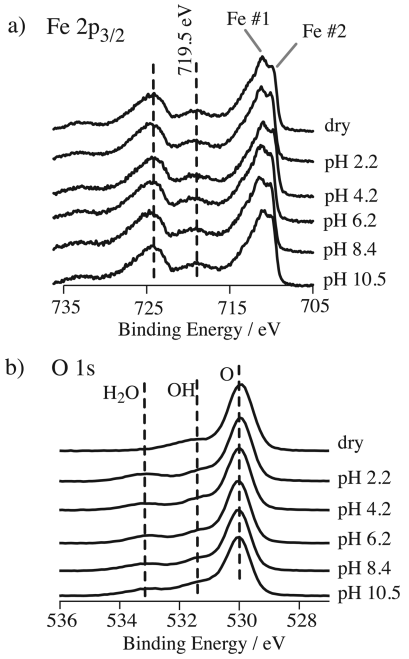

Figure 2. (a) Raw spectra of Fe $2p_{3/2}$ region in dry and wet hematite pastes. Positions of dominant peaks of hematite (Fe#1 and Fe#2) and satellites are shown. (b) Raw spectra of O 1s region with peaks from H_2O, OH, and O.

Table 2. Atomic Ratios

	O/Fe	OH/Fe	H_2O/Fe	NH_3/Fe	NH_4/Fe	N_{tot}/Fe	Cl/Fe
			No NH_4Cl				
dry	1.145	0.086	0.022				0.027
wet	0.978	0.385	0.311				0.002
			Fast-Frozen in 50 mM NH_4Cl				
pH 2.2	1.056	0.347	0.176	0.004	0.026	0.030	0.060
pH 4.2	1.049	0.327	0.166	0.007	0.018	0.025	0.048
pH 6.2	1.075	0.353	0.055	0.005	0.016	0.021	0.043
pH 8.4	1.067	0.305	0.155	0.017	0.019	0.036	0.029
pH 10.5	1.052	0.355	0.133	0.020	0.010	0.029	0.019
			Dried in Vacuo				
pH 6.2	1.003	0.128	0.008	0.017	0.010 (NH_2)	0.026	0.045

(Figure 1, Tables 1 and 2) in terms of binding energies, intensities, and fwhm values. Associated MCR concentration profiles (Figure 4) are also in strong agreement with relative peak area obtained by peak-fitting and thereby provide additional support for coexisting NH_4^+ and NH_3 species over almost the entire pH 2.2−10.5 range.

Both peak-fitting and MCR analyses underscore important differences in ammonia speciation in water and in hematite wet pastes. The N concentration profiles in these pastes are, in particular, considerably different than those of water, where NH_4^+ and NH_3 species should coexist only within 1 pH unit about the pK_a of 9.3 (Figure 4). As binding energies of NH_4^+ and NH_3 are identical in both aqueous solutions and hematite wet pastes, and N loadings are not correlated to those of H_2O (Table 2), these differences cannot be explained by strong

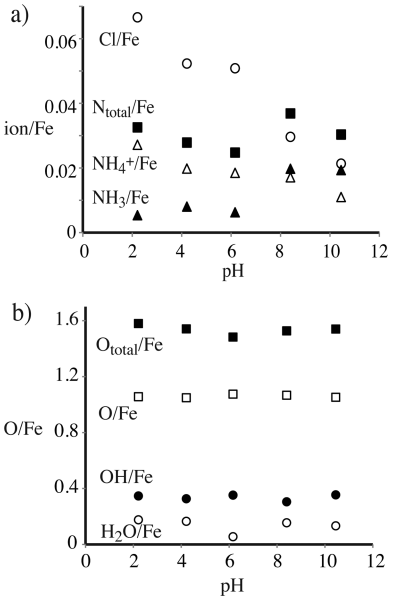

Figure 3. Atomic percentages normalized for Fe: (a) N and Cl electrolyte species; (b) oxygen species.

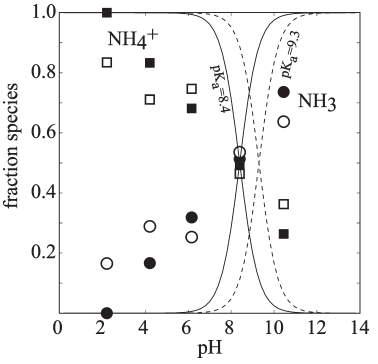

Figure 4. Speciation and surface loading of N on hematite. Values for NH_4^+ (■, □) and NH_3 (●, ○) are shown as percent of total N. Open symbols were obtained by peak-fitting and closed symbols by MCR. Lines are predictions for aqueous speciation ($NH_4 \rightleftarrows NH_3 + H^+$ pK_a) with pK_a = 9.3 (dashed) and pK_a = 8.4 (full).

changes in hydrogen-bonding strength with water. The broader range of pH values where these species coexist and the increased acidity of ammonium (pH of intersection = pK_a = 8.4) are rather indicative of surface-mediated effects. Lack of structural and oxidation change in hematite and the predominance of oxygen-terminated surfaces (O_{Total}/Fe = 1.48−1.69) moreover point to N interactions with surface (hydr)oxo groups.

Experimental results to be published in the following article of this series provide clear evidence for highly comparable sorption edges between NH_3 and a range of alkali metal ions (Na^+, K^+, Rb^+, Cs^+). This similarity underscores a strong correlation between NH_3 sorption and the development of negatively charged (hydr)oxo species of the hematite surface. Recalling that hydrogen bonding is a predominant gas-phase adsorption mechanism for the ammonium ion,[8,9] abstraction of a proton from NH_4^+ by (hydr)oxo groups, resulting in a complex of the type $\equiv Fe_x{-}OH_y\cdots NH_3$, could be a driving force for the cationic sorption edge of NH_3 and for the decrease in pK_a.

dx.doi.org/10.1021/jp2002035 |J. Phys. Chem. C 2011, 115, 6796–6801

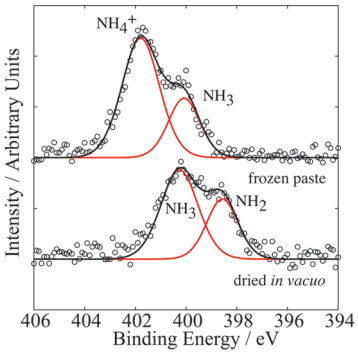

Figure 5. N 1s spectra of hematite treated in 50 mM NH_4Cl at pH 6.2, first analyzed as a fast-frozen paste and then dry after warming up to room temperature. Peaks of NH_4^+ and NH_3 occur at 401.7 and 400.0 eV, respectively, in the frozen paste. The dry solid exhibits, on the other hand, peaks from NH_3 and NH_2 at 400.2 and 398.5 eV, respectively.

Interestingly as N/Fe loadings are largely pH independent, NH_4^+ must also be stabilized by the hematite surface. Stabilization of this positively charged species follows typical proton sorption isotherms and may consequently involve hydrogen bonding ($\equiv Fe_x-OH_y\cdots HNH_3$) with the same surface (hydr)oxo groups.

Stabilization of ammonium species at the hematite/water interface does not, as in the gas phase, result in metal-bonded (Fe−N) species. Formation of such species may in fact be prevented by an insufficiently strong drive for ligand exchange reactions. Formation of Fe−N bonds could consequently necessitate removal of surface-bound OH/H_2O by drying. To illustrate this point further, a frozen wet paste equilibrated at pH 6.2 was dried in vacuo by warming to room temperature. As expected, associated loss and exposure of the hematite to vacuum induced oxygen-deficient surfaces ($O_{Total}/Fe = 1.14$) (Table 2). The N 1s region underwent substantial change with the complete disappearance of the 401.7 eV (NH_4^+) peak and the appearance of a peak at 398.5 eV (Figure 5). Comparisons with previous studies also showing comparable binding energy difference (1.5 eV) between these two peaks (e.g., Cr_2O_3 (2.1 eV)[35] and NiO (1.9 eV)[36]) support formation of dehydrogenated ammonia species (NH_2) and the formation of direct Fe−N interactions. Plausible reactions involving dehydration-induced conversion of NH_4^+ to NH_3 ($\equiv Fe_x-OH\cdots HNH_3 \rightarrow \equiv Fe_x-NH_3 + H_2O$) and NH_3 to NH_2 ($\equiv Fe_x-OH\cdots NH_3 \rightarrow \equiv Fe_x-NH_2 + H_2O$) may be responsible for these important spectral changes. Although these dehydration-induced changes warrant further substantiation using complementary techniques (e.g., vibration spectroscopy), the absence of dehydrogenated species in frozen wet samples supports predominance of hydrogen bonding between ammonium species and hydroxyl functional groups of the hematite surface.

4. CONCLUSIONS

Hematite colloids in contact with aqueous solutions of ammonium chloride acquire pH invariable surface loadings distributed as NH_4^+ and NH_3 species. Both species are stabilized by (hydr)oxo functional groups of the hematite surface. Interactions with these groups facilitate proton dissociation from NH_4^+, compared to fully dissolved aqueous species. The affinity of these species to hematite/water interfaces, and most possibly to hydrated interfaces of other metal oxides, is driven by their ability in forming hydrogen bonds with oxygen moieties. Given the water-breaking attributes of ammonia species, important changes in water structures may be induced at the hematite/water interface. This may have important repercussions on processes including sorption mechanisms, water exchange, catalytic reactivity, as well as colloidal stability and transport. Our work represents a first line of evidence supporting the presence of such species at the hematite/water interface and calls for further experimental (e.g., X-ray reflectivity, vibration spectroscopy) and theoretical (e.g., molecular dynamics, ab initio) work probing potentially altered physicochemical properties, such as interfacial water structures.

■ ASSOCIATED CONTENT

Supporting Information. Transmission electron microscopy imaging of hematite particles, wide XPS spectra, and chemometric analyses of the N 1s region. This material is available free of charge via the Internet at http://pubs.acs.org.

■ AUTHOR INFORMATION

Corresponding Author

*E-mail: jean-francois.boily@chem.umu.se; tel: +46 90 786 5270.

■ ACKNOWLEDGMENT

This work was supported by the Swedish Research Council (2009-34104-69231-39), as well as the Wallenberg, Kempe, and Carl Tryggers Foundations.

■ REFERENCES

(1) Bockris, J. O. M.; Khan, S. U. M. *Surface Electrochemistry. A Molecular Level Approach*: Plenum Press: New York, 1993.

(2) Israelachvili, J. N. *Intermolecular and Surface Forces*; Academic: London, U.K., 1992.

(3) Sverjensky, D. A. Prediction of Surface Charge on Oxides in Salt Solutions: Revisions for 1:1 (M^+L^-) Electrolytes. *Geochim. Cosmochim. Acta* **2005**, *69*, 225.

(4) Intharathep, P.; Tongraar, A.; Sagarik, K. Structure and Dynamics of Hydrated NH_4^+: An *ab Initio* QM/MM Molecular Dynamics Simulation. *J. Comput. Chem.* **2005**, *26*, 1129.

(5) Brugé, F.; Bernasconi, M.; Parrinello, M. *Ab Initio* Simulation of Rotational Dynamics of Solvated Ammonium Ion in Water. *J. Am. Chem. Soc.* **1999**, *121*, 10883.

(6) Perrin, C. L.; Gipe, R. K. Rotation and Solvation of Ammonium Ion. *Science* **1987**, *238*, 1393.

(7) Perrin, C. L.; Gipe, R. K. Rotation, Solvation, and Hydrogen Bonding of Aqueous Ammonium Ion. *J. Am. Chem. Soc.* **1986**, *108*, 1088.

(8) Zecchina, A.; Marchese, L.; Bordiga, S.; Pazè, C.; Gianotti, E. Vibrational Spectroscopy of NH_4^+ Ions in Zeolitic Materials: An IR Study. *J. Phys. Chem. B* **1997**, *101*, 10128.

(9) Hasegawa, T.; Shirotori, Y.; Ozawa, K.; Edamoto, K.; Takahashi, K. Room Temperature Adsorption of NH_3 on Zn-Terminated ZnO-(001). *Appl. Surf. Sci.* **2004**, *237*, 352.

(10) Erdogan, R.; Ozbek, O.; Onal, I. A. Periodic DFT Study of Water and Ammonia Adsorption on Anatase TiO_2 (001) Slab. *Surf. Sci.* **2010**, *604*, 1029.

(11) Onal, I.; Soyer, S.; Senkan, S. Adsorption of Water and Ammonia on TiO_2−Anatase Cluster Model. *Surf. Sci.* **2006**, *600*, 2457.

(12) Park, C.; Fenter, P. A.; Nagy, K. L.; Sturchio, N. C. Hydration and Distribution of Ions at the Mica−Water Interface. *Phys. Rev. Lett.* **2006**, *97*, 016101.

(13) Zhang, Z.; Fenter, P.; Cheng, L.; Sturchio, N. C.; Bedzyk, M. J.; Predota, M.; Bandura, A.; Kubicki, J. D.; Lyov, S. N.; Cummings, P. T.;

Chialvo, A. A.; Ridley, M. K.; Benezeth, P.; Anovitz, L.; Palmer, D. A.; Machesky, M. L.; Wesolowski, D. J. Ion Adsorption at the Rutile−Water Interface: Linking Molecular and Macroscopic Properties. *Langmuir* **2004**, *20*, 4954.

(14) Zang, Z.; Fenter, P.; Sturchio, N. C.; Bedzyk, M. J.; Machesky, M. L.; Anovitz, L. M.; Wesolowski, D. J. Zn^{2+} and Sr^{2+} Adsorption at the TiO_2(110)−Electrolyte Interface: Influence of Ionic Strength, Coverage, and Anions. *J. Colloid Interface Sci.* **2006**, *295*, 50.

(15) Shchukarev, A.; Boily, J.-F.; Felmy, A. R. XPS of Fast Frozen Hematite Colloids in NaCl Aqueous Solutions. I. Evidence for the Formation of Multiple Layers of Hydrated Sodium and Chloride Ions Induced by the {001} Basal Plane. *J. Phys. Chem. C* **2007**, *111*, 18307.

(16) Boily, J.-F.; Shchukarev, A. X-ray Photoelectron Spectroscopy of Fast-Frozen Hematite Colloids in Aqueous Solutions. 2. Tracing the Relationship between Surface Charge and Electrolyte Adsorption. *J. Phys. Chem. C* **2010**, *114*, 2613.

(17) Shchukarev, A.; Sjöberg, S. XPS with Fast-Frozen Samples: A Renewed Approach to Study the Real Mineral/Solution Interface. *Surf. Sci.* **2005**, *584*, 106.

(18) Shchukarev, A.; Boily, J. F. XPS Study of the Hematite−Aqueous Solution Interface. *Surf. Interface Anal.* **2008**, *40*, 349.

(19) Ramstedt, M.; Andersson, B. M.; Shchukarev, A.; Sjöberg, S. Surface Properties of Hydrous Manganite (γ-MnOOH). A Potentiometric, Electroacoustic, and X-ray Photoelectron Spectroscopy Study. *Langmuir* **2004**, *20*, 8224.

(20) Cornell, R. M.; Schwertmann, U. *The Iron Oxide*, 2nd ed.; Wiley-VCH: Weinheim, Germany, 2003.

(21) Sadykov, V. A.; Isupova, L. A.; Tsybulya, S. V.; Cherepanova, S. V.; Litvak, G. S.; Burgina, E. B.; Kustova, G. N.; Kolomiichuk, V. N.; Ivanov, V. P.; Paukshtis, E. A.; Golovin, A. V.; Avvakumov, E. G. Effect of Mechanical Activation on the Real Structure and Reactivity of Iron(III) Oxide with Corundum-Type Structure. *J. Solid State Chem.* **1996**, *123*, 191.

(22) Malinowski, E. R. Determination of Number of Factors and Experimental Error in a Data Matrix. *Anal. Chem.* **1977**, *49*, 612.

(23) Boily, J.-F.; Gassman, P. L.; Peretyazhko, T.; Szanyi, J.; Zachara, J. M. FTIR Spectral Components of Schwertmannite. *Environ. Sci. Technol.* **2010**, *44*, 1185.

(24) Boily, J.-F.; Ilton, E. S. An Independent Confirmation of the Correlation of Uf4 Primary Peaks and Satellite of U^{VI}, U^{V}, and U^{IV} in Mixed Valence Uranium Oxides by Two-Dimensional Correlation Spectroscopy. *Surf. Sci.* **2008**, *602*, 3637.

(25) Boily, J.-F.; Felmy, A. R. On the Protonation of Oxo- and Hydroxo- Groups of the Goethite (α-FeOOH) Surface: A FTIR Spectroscopic Investigation of Surface O−H Stretching Vibrations. *Geochim. Cosmochim. Acta* **2008**, *72*, 3338.

(26) Boily, J.-F.; Qafoku, O.; Felmy, A. R. A Potentiometric, Spectrophotometric and Pitzer Ion-Interaction Study of Reaction Equilibria in the Aqueous H^{+}-Al^{3+}, H^{+}-Oxalate, and H^{+}-Al^{3+}-Oxalate Systems up to 5 mol·dm^{-3} NaCl. *J. Solution Chem.* **2007**, *36*, 1727.

(27) Ilton, E. S.; Boily, J.-F.; Bagus, P. Beam Induced Reduction of U(VI) during X-ray Photoelectron Spectroscopy: The Utility of the U4f satellite Structure for Identifying Uranium Oxidation States in Mixed Valence Uranium Oxides. *Surf. Sci.* **2007**, *601*, 908.

(28) Boily, J.-F.; Seward, T. M. Palladium(II) Chloride Complexation: Spectrophotometric Investigation in Aqueous Solutions from 5 to 125°C and Theoretical Insight into Pd−Cl and Pd−OH_2 Interactions. *Geochim. Cosmochim. Acta* **2005**, *69*, 3773.

(29) Jaumot, J.; Gargallo, R.; de Juan, A.; Tauler, R. A Graphical User-Friendly Interface for MCR-ALS: A New Tool for Multivariate Curve Resolution in MATLAB. *Chemometrics Intell. Lab. Syst.* **2005**, *76*, 101.

(30) Droubay, T.; Chambers, S. A. Surface-Sensitive Fe 2p Photoemission Spectra for α-Fe_2O_3 (0001): The Influence of Symmetry and Crystal-Field Strength. *Phys. Rev. B.* **2001**, *64*, 205414.

(31) Siew, H. L.; Qiao, M. H.; Chew, C. H.; Mok, K. F.; Chan, L.; Xu, G. Q. Adsorption and Reaction NH_3 on Ti/Si (100). *Appl. Surf. Sci.* **2001**, *173*, 95.

(32) Ramstedt, M.; Norgren, C.; Sheals, J.; Shchukarev, A.; Sjöberg, S. Chemical Speciation of *N*-(Phosphonomethyl)glycine in Solution and at Mineral Interfaces. *Surf. Interface Anal.* **2004**, *36*, 1074.

(33) Sheals, J. *Molecular Characterisation of Glyphosate Complexes in Aqueous Solution and at the Solution−Mineral Interface*. Ph.D. Thesis, Umeå University, 2002

(34) Mladenovic, Z.; Sahlin-Platt, A.; Ransjö, M.; Shchukarev, A. Surface Characterization of Bone Graft Substitute Materials Conditioned in Cell Culture Medium. *Surf. Interface Anal.* **2010**, *42*, 452.

(35) Ma., H.; Berthier, Y.; Marcus, P. AES, XPS, and TDS study of the Adsorption and Desorption of NH_3 on Ultra-Thin Chromium Oxide Films Formed on Chromium Single Crystal Surfaces. *Appl. Surf. Sci.* **1999**, *153*, 40.

(36) Galtayries, A.; Laksono, E.; Siffre, J.-M.; Argile, C.; Marcus, P. XPS Study of the Adsorption of NH_3 on Nickel Oxide on Ni(111). *Surf. Interface Sci.* **2000**, *30*, 140.